International Journal of Mechanical and Production Engineering Research and Development (IJMPERD)
ISSN (P): 2249-6890; ISSN (E): 2249-8001
Vol. 9, Issue 4, Aug 2019, 317-332

TRANS STELLAR
•Journal Publications •Research Consultancy

A CUSTOMIZED WAVELET-BASED HIERARCHICAL *A POSTERIORI* ERROR INDICATOR FOR LINEAR AND NONLINEAR PDEs

KUMAR KAUSHIK RANJAN, AMBUJ SHARMA, SANDEEP KUMAR & AMIT TYAGI

Department of Mechanical Engineering, IIT(BHU), Varanasi, India

ABSTRACT

This paper presents an adaptive method that can be used to improve the finite element solution of a linear or non-linear PDE by indicating the local as well as global errors. This wavelet-based adaptation is based on hierarchical finite element error estimation scheme. The finite element solution of engineering problems is transformed into the multilevel decomposition of wavelet space. The functions of wavelets coefficient are used as an a posteriori error indicator. The error estimations in the present setting do not have any problem due to the complex domain of engineering structures and is applicable in some small region as well as the complete domain. The proposed technique is quite efficient for linear problems like structures with discontinuity as well as non-linear ones such as contact problem.

KEYWORDS: Finite Element Method, Aposteriori Error Estimator, Multi-Resolution Analysis & Second Generation Wavelets

Received: May 01, 2019; **Accepted**: May 22, 2019; **Published**: Jun 25, 2019; **Paper Id.**: IJMPERDAUG201933

Original Article

1. INTRODUCTION

There is no analytic theory for mesh refinement for most of the boundary value problems (BVP). Therefore, the adaptive mesh cannot be generated to improve the solution on the basis of any prior information. *A posteriori* error estimate is a key ingredient for improving the accuracy of the solution in the successive iteration. The adaptive mesh generation process depends on the successful application of *a posteriori* error estimation techniques which is not only a tool for grid optimization but also provide the estimate of the error in the current numerical solution. There exists a vast literature on various error estimation techniques [1-12] which are recently developed. Most of the estimators use local quantities such as jump of derivatives across the interface between two adjacent elements[13–18]. The residuals due to local quantities are used for estimating upper and lower bounds of the global error in terms of energy norm. The quality of estimated error by using canonical error-estimation techniques depends on the initial mesh which is often overestimated.

The hierarchical approach, which is a multi-scale expansion[19-20]of corresponding FEM, is often used for *a posteriori* error estimate due to its simplicity and effectiveness[21-22]. The hierarchical basis functions span the space of traditional basis functions of finite element method, and it has desirable properties for fast iterative solvers. *A posteriori* error in the hierarchical approach is represented as a convergent sequence of errors of the Hilbert space. In other words, unlike the other classical error estimators which use total error within an element as an indicator, the higher level component is used as an indicator in this scheme. It is noted that such *a posteriori* error estimators are useful in identifying local as well as global error.

The hierarchical basis functions are defined as “lazy wavelets”[23]. The hierarchical scheme has been applied to various types of partial differential equations, but wavelet-based techniques are not used frequently. Classical wavelets have many desirable properties such as orthogonality and vanishing moments which do not exist in a hierarchical basis. Bertoluzza used wavelet-based error estimator for wavelet Galerkin method. A good mathematical theory for error estimation and adaptive solution of PDEs using wavelet basis are developed[25,26]. Implementation of these wavelet-based methods is difficult on the wide range of complex boundary value engineering problems. Sudarshan[27] et al have used wavelet-based *a posteriori* error estimation for engineering structures, but this method requires customized wavelets. It is very difficult to develop customized wavelets, which should be as efficient as FEM for various types of partial differential equations.

The present work is based on the hierarchical error estimation technique proposed by Bank[28]. It combines the strength of a wavelet transform and hierarchical error estimation technique and finds the error in the finite element solution. In this method, the solution of the finite element method is transformed into the multi-resolution wavelet space using a linear transformation. For a single variable system, the detail coefficients are used as a local error indicator but some functional of detail coefficients is to be used for multiple variable problems. In the case of variational inequalities, we solve a problem that satisfies the assumptions made for the linear case and calculated the error bounds defined by Kornhuber et al[29].

2. WAVELET-BASEDERROR ESTIMATION

Consider a partial differential equation $Lu = f$ in Ω and boundary conditions $Bu = g$. The problem is to find the exact solution $u \in \mathcal{H}$. The variational form of the equation can be expressed as

$$a(u,v) = f(v) \tag{1}$$

Forall $v \in \mathcal{H}$, where $\mathcal{H}$ is an appropriate Solve space, $a(.,.)$ is a positive definite bilinear form, and $f(.)$ is linear functional. The energy norm associated with $a(.,.)$ can be defined as:

$$\|u\|^2 = a(u,u). \tag{2}$$

The best available option to solve (1) is the finite element method, and the current solution is assumed as the highest resolution for the wavelet space $u_j \in V_j \subset \mathcal{H}$. This approximate solution process introduces numerical error

$$e = u - u_j. \tag{3}$$

Obtaining the exact error e is as difficult as finding the exact solution. Thus, various indicators for *a posteriori* error estimations are developed. If the estimated error is larger than a predefined tolerance, then a re-meshing is used on the finite element grid either selectively on element with large errors or on the whole domain (uniform refinement). This is essential to form a strategy of adaptive mesh for the improvement of the solution in the successive iteration.

A brief introduction of wavelets will be useful for this error estimation technique. The concept of multi-scale analysis is to interpolate an unknown field at a coarse level with the help of so-called scaling functions. Any improvement to the initial approximation is achieved by adding ‘details’ provided by new functions known as wavelets.

A multiscale analysis uses multire solution properties of wavelets[30]. Each subspace V_j is spanned by a set of scaling function $\{\phi_{j,k}(x), \forall k \in Z\}$. The complement of V_j in V_{j+1} is defined as subspace W_j such that $V_{j+1} = V_j \oplus W_j$ for all $j \in Z$. Space V_{j+1} can be decomposed in a consecutive manner as:

$$V_{j+1} = V_0 \oplus W_0 \oplus W_1 \oplus W_2 ... \oplus W_j \ . \tag{4}$$

The basic functions in W_j are called wavelet functions and are denoted by $\psi_{j,k}$. Let $V_j \subset L^2(\Omega)$ be a finite dimensional subspaces, and consider the approximate solution $u_j \in V_j$ such that $a(u_j, v) = f(v)$ for all $v \in V_j$. Its solution holds the approximation property $\|u - u_j\| = \inf_{v \in V_j} \|u - v\|$. Similarly, for $V_j \subset V_{j+1} \subset L^2(\Omega)$ Galerkin solution $u_{j+1} \in V_{j+1}$ will satisfy $a(u_{j+1}, v) = f(v)$ for all $v \in V_{j+1}$. Here $\|u - u_j\| \to 0$, as $j \to \infty$.

Let us assume that as compared u_j the next scale refined solution u_{j+1} is closer to u. Thisis definedin terms of the saturation assumption

$$\|u - u_{j+1}\| \le \xi \|u - u_j\|, \tag{5}$$

Where $\xi < 1$. The characteristic length of a mesh element $h \to 0$ as $j \to \infty$. For a higher degree of approximation in the space V_{j+1}, Bank [21]estimated $\xi = O(h^r)$ for some $r > 0$. For $v_{j+1} \in V_{j+1}$ the unique decomposition $v_{j+1} = v_j + w_j$, where $v_j \in V_j$ and $w_j \in W_j$, we assume a strengthened Cauchy inequality for the decomposition,

$$\left|a(v_j, w_j)\right| \le \hat{\lambda} \|v_j\| \|w_j\|, \tag{6}$$

Where $\hat{\lambda} < 1$ is independent of j.

Instead of (3), Bank [21]used two-scale error in the multi-resolution approach

$$r_j = u_{j+1} - u_j. \tag{7}$$

Where $r_j \in W_j$, it means that two-level error is the projection of true error onto the wavelet space. It is proved [21]that

$$c_1 \|u - u_j\| \le \|r_j\| \le c_2 \|u - u_j\|. \tag{8}$$

Where $c_1, c_2 > 0$ are constants and independent of the multi-resolution level j. The orthogonality property [26]

$$\|u - u_j\|^2 = \|u - u_{j+1}\|^2 + \|u_{j+1} - u_j\|^2, \tag{9}$$

The saturation property is used to get the lower bounds $c_1 = \left(1-\xi^2\right)$. The two scale error will always be less than the total error, i. e. $\left\|r_j\right\| \le \left\|u-u_j\right\|$. Therefore, the two-level error is a good estimate of the actual error. Since w_j is the projection of r_j hence

$$\left\|w_{j+1}\right\| \le \left\|r_{j+1}\right\| \le \left\|w_j\right\| \le \left\|r_j\right\| \le \left\|u-u_j\right\|. \tag{10}$$

The two consecutive levels of FEM refinements can be used to calculate two scale error $\left\|r_{j+1}\right\|$ or $\left\|r_j\right\|$. This method is expensive to estimate error. Therefore FE solution is transformed using discrete wavelets. The norm of some functional calculated using wavelet coefficients shows a sudden jump in some areas which indicate the need for mesh refinement in that zone. The cost of computing $\left\|w_{j+1}\right\|$ or $\left\|w_j\right\|$ is considerably less than the two scale error.

Theorem

Let $V_{j+1} = V_j \oplus W_j$, strengthen Cauchy inequality and saturation property holds then

$$\left(1-\xi^2\right)\left(1-\lambda^2\right)\left\|u-u_j\right\|^2 \le \left\|w_j\right\|^2 \le \left\|u-u_j\right\|^2.$$

Proof

The proposed posteriori error estimate $w_j \in W_j$ is the error of the solution $u_j \in V_j$ such that

$$a\left(w_j, v\right) = f\left(v\right) - a\left(u_j, v\right) \;\forall\; v \in W_j$$

$$\text{or, } a\left(u-u_j-w_j, v\right) = 0 \qquad \forall\; v \in W_j. \tag{11}$$

Substitution of $v = w_j$ in the preceding equation gives right inequality of the theorem. Let $u_{j+1} = \hat{u}_j + \hat{w}_j$ where $\hat{u}_j \in V_j$ and $\hat{w}_j \in W_j$ then

$$\left\|u_{j+1}-u_j\right\|^2 = \left\|\hat{u}_j + \hat{w}_j - u_j\right\|^2$$

$$\ge \left\|\hat{u}_j - u_j\right\|^2 + \left\|\hat{w}_j\right\|^2 - 2\lambda\left\|\hat{u}_j - u_j\right\|\left\|\hat{w}_j\right\|$$

$$\ge \left\|\hat{u}_j - u_j\right\|\left(\lambda\left\|\hat{w}_j\right\| - 2\lambda\left\|\hat{w}_j\right\|\right) + \left\|\hat{w}_j\right\|^2$$

$$\ge \left(1-\lambda^2\right)\left\|\hat{w}_j\right\|^2. \tag{12}$$

By using orthogonality relations $a\left(u-u_j,v\right)=0\ \forall\ \ v\in V_j$ and $a\left(u-u_{j+1},v\right)=0\ \forall\ \ v\in V_{j+1}$, we get $a\left(u_{j+1}-u_j,v\right)=0\ \forall\ \ v\in V_j$. Substitution of $v=\hat{u}_j-u_j$, gives

$$\left\|u_{j+1}-u_j\right\|^2=a\left(u_{j+1}-u_j,\hat{w}_j\right). \tag{13}$$

On subtracting (11) from $a\left(u-u_{j+1},v\right)=0\ \forall\ \ v\in V_{j+1}$, we get $a\left(u_{j+1}-u_j-w_j,v\right)=0 \quad \forall\ \ v\in W_j$.

With $v=\hat{w}_j$, we get

$$a\left(u_{j+1}-u_j,\hat{w}_j\right)=a\left(w_j,\hat{w}_j\right). \tag{14}$$

Using (13) and (14), we have

$$\left\|u_{j+1}-u_j\right\|^2=a\left(w_j,\hat{w}_j\right).$$

Using (6) in the preceding equation, it can be shown that

$$\left\|u_{j+1}-u_j\right\|^2\le\left\|w_j\right\|\left\|\hat{w}_j\right\|. \tag{15}$$

From (12) and (15) we obtain

$$\left\|w_j\right\|\ge\left(1-\lambda^2\right)\left\|\hat{w}_j\right\|. \tag{16}$$

On substituting (15) in (9), we get

$$\left\|u-u_j\right\|^2=\left\|u-u_{j+1}\right\|^2+\left\|w_j\right\|\left\|\hat{w}_j\right\|$$

Using saturation assumption, we obtain

$$\left\|u-u_j\right\|^2\le\xi^2\left\|u-u_j\right\|^2+\left\|w_j\right\|\left\|\hat{w}_j\right\|.$$

Combining this with (16), we have

$$\left(1-\xi^2\right)\left\|u-u_j\right\|^2\le\frac{1}{1-\lambda^2}\left\|w_j\right\|^2$$ □

3. ESTIMATION OF WAVELET COEFFICIENTS

Now we have to determine the error in a computationally efficient way. In this paper, we used the functional of wavelet coefficients. A function $u_{j+1}\in L^2(R)$ is approximated by its projection P^ju_j onto the space V_j and the projection on W_j as Q^ju_j,

$$P^{j+1}u_{j+1} = P^{j}u_{j} + Q^{j}u_{j}.$$

The coefficient vector $u_j = \{u_{j,0}, \ldots\ldots, u_{j,\upsilon(j)}\}^T$ of some scaling function basis forms the projection $P^j u_j$ and $w_j = \{w_{j,0}, \ldots\ldots, w_{j,\omega(j)}\}^T$ of some wavelet forms the matrix $Q^j u_j$. The approximate solution $u_j \in V_j \subset V$ can be represented in a multi-resolution format consisting of scaling functions and compactly supported wavelets up to a resolution of j

$$u_{j+1} = \sum_k u_{0,k}\phi_{0,k} + \sum_{j=0}^{j-1}\sum_m r_{j,m}\psi_{j,m} \tag{17}$$

Here $u_{0,k}$ and $r_{j,m}$ are a projection of function u on scaling function ϕ and wavelets ψ respectively. We take ϕ to be Lagrange finite element functions and ψ as hierarchical finite element bases [31].

Considering only one level we have u_{j+1}

$$u_{j+1} = \sum_t u_{j,t}\phi_{j,t} + \sum_s r_{j,s}\psi_{j,s} \tag{18}$$

The error w_j becomes(from equation (7))

$$\| r_j \| = \| \sum_t u_{j,t}\phi_{j,t} + \sum_s r_{j,s}\psi_{j,s} - \sum_t u_{j,t}\phi_{j,t} \| \tag{19}$$

$$= \| \sum_s r_{j,s}\psi_{j,s} \|$$

To calculate the detail coefficient, we use the multi-resolution format of the trial function in the Galerkin formulation

$$a(\sum_k u_{0,k}\phi_{0,k} + \sum_{j=0}^{J-1}\sum_m r_{j,m}\psi_{j,m}, v_h) = l(v_h) \tag{20}$$

We get a multi-scale stiffness matrix in the form

$$\begin{bmatrix} S_0^s & S_{0,1}^I & \cdots & S_{0,j-1}^I \\ S_{0,1}^{I\,T} & D_1^D & \cdots & S_{1,j-1}^I \\ \vdots & \vdots & \ddots & \vdots \\ S_{0,j-1}^{I\,T} & S_{1,j-1}^{I\,T} & \cdots & D_{j-1}^D \end{bmatrix} \begin{bmatrix} u_0^s \\ r_0 \\ \vdots \\ r_{j-1} \end{bmatrix} = \begin{bmatrix} f_0^s \\ f_0^D \\ \vdots \\ f_{j-1}^D \end{bmatrix} \tag{21}$$

Here the sub-matrices S^s and D_i^D are defined as

$$S^s = a(\phi_0, \phi_0) \text{ where } \phi_0 = \{\phi_{0,k}\} \tag{22}$$

$$D_i^D = a(\psi_i, \psi_i) \text{ where } \psi_i = \{\psi_{i,k}\} \tag{23}$$

They contain interactions of scaling -scaling and wavelet-wavelet functions spanning sub-spaces of the same scale. Sub-matrices S_{j-1}^I are defined as

$$S_{i,j-1}^I = a(\phi_{i-1}, \psi_{j-1}) \tag{24}$$

They contain connection coefficients of interactions between scaling and wavelet functions. Vectors *f*, *u* and *w* represent the decomposition of load vector and the unknown solution over different scales of resolution. By solving the sub system $D_i^D r_i = f_i^D$ we can calculate the two-level error/details at a certain level i. But as the multi-resolution matrix is coupled over scales, we need to eliminate the interaction sub-matrices. The interaction sub-matrices can be eliminated by customizing the wavelet basis ψ [27]such that

$$S_{i,j-1}^I = 0 \tag{25}$$

So, the system becomes decoupled over scales. Scale decoupling of the multilevel system splits it into sub-systems that can be solved individually. Such wavelets that can decouple the multi-scale matrix are created using the second generation wavelet techniques, i. e. lifting scheme and stable completion [27].

$$\psi_{i,j} = \sum_k g_{i,k,j}\phi_{i+1,k} + \sum_m s_{i,m,j}\phi_{i,m} \tag{26}$$

Here $\psi_{i,j}$ and $\phi_{i,j}$ are the *j* th wavelet and the Lagrangian basis function, respectively at the *i* th level of resolution g and s coefficients are obtained by solving the system

$$K_{i,j'}\lambda_{i,j'} = 0 \tag{27}$$

In this equation, $K_{i,j'}$ is a block interactions sub-matrix with respect to the weak form of the desired PDE operator and is defined as

$$K_{i,j'} = a(\phi_{i,k}, \sum_k g_{i,k,j'}\phi_{i+1,k} + \sum_m s_{i,m,j'}\phi_{i,m}) \tag{28}$$

This sub-matrix occurs naturally in the multi-scale stiffness matrix of equation(21), and is composed of the inner product between *k* + *m* Lagrangian basis functions, the wavelet function $\psi_{i,j}$ and all Lagrangian basis functions that have overlapping local support on the j' th level. $\lambda_{i,j}$ is the matrix with *n* columns of *k*+*m* coefficients g and s, and *n* is the number of resulting wavelets for the level j'.

The algebraic form of the linear variational problem $a(u_j, v) = f(v)$ is

$$\text{Find } u_j \in V_j : K_j u_j = f_j \tag{29}$$

Using the multi-resolution structure of trial function, we get a multi-level stiffness matrix (equation 21). Using the

combination of equations (20),(27),(28) some multi-scale system matrix (equation 21) can be block diagonalized

$$\begin{bmatrix} S_0^s & & \cdot & \\ & D_1^D & \cdot & \cdot \\ \cdot & \cdot & \ddots & \cdot \\ & \cdot & \cdot & D_{j-1}^D \end{bmatrix} \begin{bmatrix} u_0^s \\ r_0 \\ \vdots \\ r_{j-1} \end{bmatrix} = \begin{bmatrix} f_0^s \\ f_0^D \\ \vdots \\ f_{j-1}^D \end{bmatrix} \tag{30}$$

The first sub-system

$$S_0^s u_0^s = f_0^s \tag{31}$$

will produce the initial approximate solution of low accuracy, and is same as the finite element solution obtained in a coarsely discretized mesh. Solution of subsystem

$$D_1^D r_0 = f_0^D \tag{32}$$

results in details belonging to wavelets of scale 1. The details are then combined with the coarse scale solution, providing the improved solution. We continue the refinement process until the desired accuracy is reached.

The detail coefficient computed at each level of resolution is the difference between two successive solutions, so it iscalled as a two-level error. Use of wavelet-based error estimation doesn't require post-processing of results. The other methods of error estimation require an evaluation of specific equations on an element by element basis.

4. NUMERICAL EXPERIMENTS

We developed the wavelet-basedcost-effective error indicator. To test the performance of proposed error estimators, we compare it with exact error and two scale error indicator for standard problems. In the first example, we consider the linear initial-boundary value hyperbolic problem:

$$\frac{\partial u}{\partial t} - y\frac{\partial u}{\partial x} + x\frac{\partial u}{\partial y} = 0,\ -1.2 \le x,\ y \le 1.2,\ t > 0,$$

and initial conditions $u(x,y,0) = \begin{cases} 0 & \text{if } (x\text{-}0.5)^2 + 1.5y^2 \ge 0.0625 \\ 1 - 16((x-0.5)^2 + 1.5y^2) & \text{otherwise.} \end{cases}$

The Dirichlet boundary conditions on all four sides $u(1.2,y,t) = u(-1.2,y,t) = u(x,-1.2,t) = u(x,1.2,t) = 0$ are considered. The solution to this problem is a moving elliptical cone that rotates counterclockwise direction around the origin with a period π. It can be written in the form $u(x,y,t) = \begin{cases} 0 & \text{if } C < 0 \\ C & \text{if } C \ge 0, \end{cases}$ where

$C = 1 - 16[(x\cos t + y\sin t - 0.5)^2 + 1.5(y\cos t + x\sin t)^2].$

The equation is solved by using finite element method for various level of uniform mesh. At $0 < t \le 3.2$, the New mark time integration scheme is used with a time step Δt = 0.00625 s.

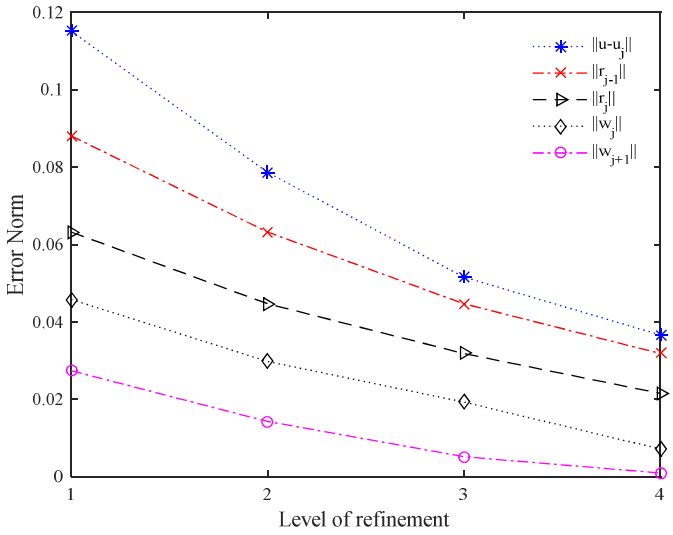

Figure 1: Comparison of Exact, Two Scales, and Proposed Error Estimators

Figure 1 shows the errors $\|u-u_j\|$, $\|r_j\|$ and the proposed estimator $\|w_j\|$ with the increasing degrees of freedom. Initially at $j=1$, a uniform grid of 20×20 is used. The grid is doubled at every successive level j for multi-scale wavelets. The figure shows the convergence of exact error as the degrees of freedom increases. It can be observed that the two-level indicator and the proposed indicator show the similar trend of convergence of global error with the level of refinement. This ensures the reliability of the proposed wavelet-based estimator.

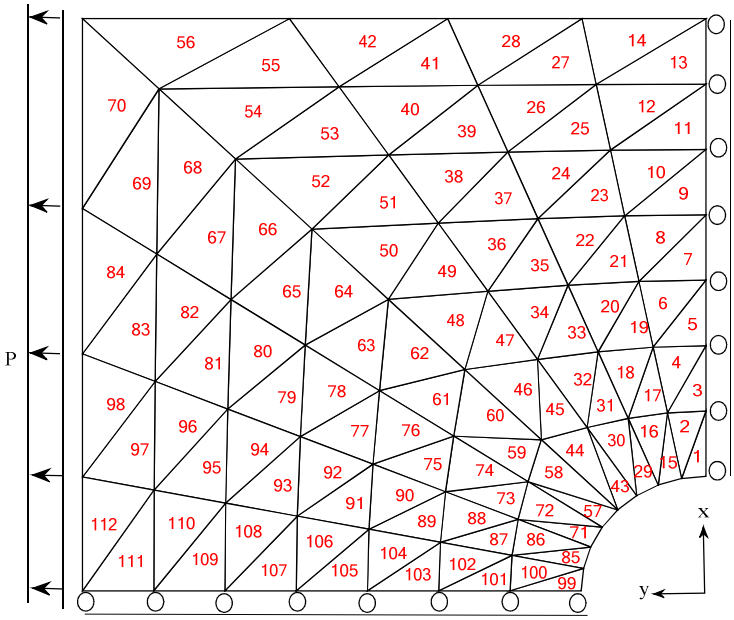

Figure 2: One-Quarter of the Discretized Rectangular Plate with a Hole

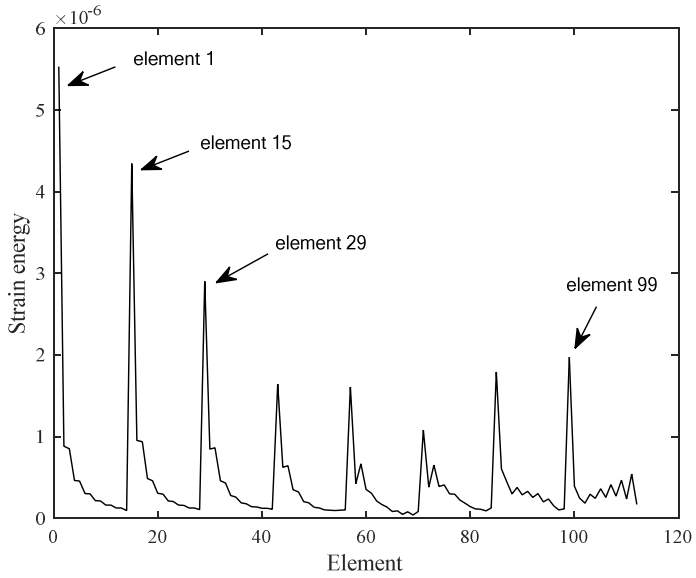

Figure 3: Strain Energy using Two Scale Difference

To demonstrate the effectiveness of the two-level error indicator and proposed error indicator for local error estimation, both the methods are tested on a standard 2D linear elasticity problem. The zone of mesh refinement for a plate with a hole under longitudinal tensile loading is very well known. Both the error indicators are tested by considering one-fourth of the plate as shown in Figure 2. The regions of interest in these problems are the elements in the neighborhood of the circular hole where stress concentration is very high. The functional used for two-level error indicator is the difference of strain energy at two consecutive levels of finite element solutions. The peaks in the Figure 3, indicates the elements with high local error i. e., these elements are to be refined. For the proposed error indicator, the strain energy is calculated by using wavelet coefficients and shown in Figure 4. As in the previous example, we see the similar peaks at high-stress concentration elements, but the proposed error indicator is much more economical than the two-level error indicator. Convergence of stress is used to stop the refinement process.

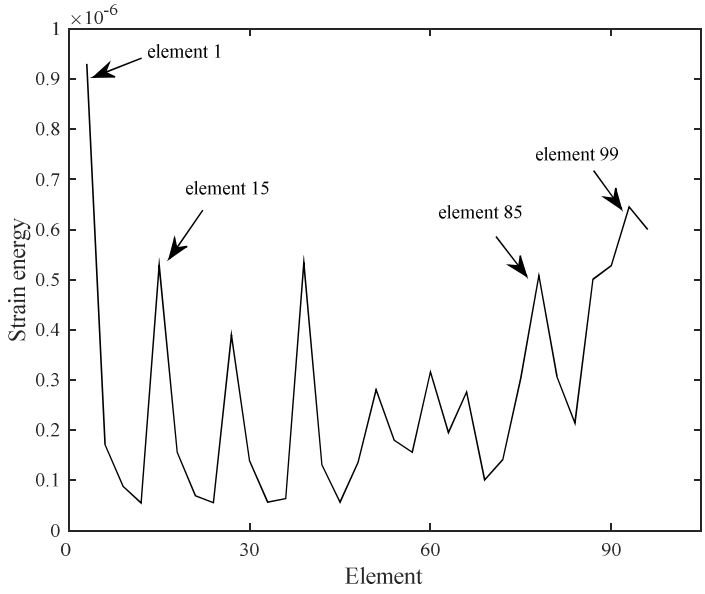

Figure 4: Strain Energy using Wavelet Coefficient

As an on-linear example, we consider the contact problem that is a variational inequality of the first kind. The governing differential equation of contact can be written in the strong form as

$$-\nabla(\mathbf{C}:\varepsilon(u)) = f \text{ in } \Omega \tag{33}$$

$u = 0$ on Γ_D,

$\sigma\mathbf{n} = t$ on Γ_N,

$u^T\mathbf{n} \le g$ and $\mathbf{n}^T\sigma\mathbf{n} \ge 0$ on Γ_C.

Here Γ represents the boundary of the domain, with $\Gamma_C, \Gamma_D, \Gamma_N$ representing the contact, Dirichlet, and Neumann boundaries respectively($\Gamma_C \cup \Gamma_D \cup \Gamma_N = \Gamma$) with g defined as gap function and $\mathbf{n}$ is the unit normal along the contact boundary.

The inequality is written in the bilinear form as

$$a(u, v-u) \ge l(v-u)\ \forall v \in \mathrm{K} \tag{34}$$

K is defined as a closed and convex set of permissible functions $\mathrm{K} = \{v \in \prod_j H_0^1(\Omega_j) | \boldsymbol{v}.\boldsymbol{n} \le g\}$

We discretize (34) using $\phi_j \in V_j$ such that a finite-dimensional dimensional problem is obtained

$$u_j \in \overline{\mathrm{K}}_j : a(u_j, v_j - u_j) \ge l(v_j - u_j)\ \forall v_j \in \overline{\mathrm{K}}_j \tag{35}$$

With $\overline{\mathrm{K}}_j$ given as $\left\{ \overline{\mathrm{K}}_j = \mathrm{v} \in \prod_j \mathrm{V_j}(\Omega_j) | \int_{\Gamma_c} \boldsymbol{v}.\boldsymbol{n}\,\mu_j\,ds \le \int_{\Gamma_c} (g - \boldsymbol{u_j}.\boldsymbol{n})\,\mu_j ds, \forall \mu \in M_j \right\}$

Here M_j is the cone of Lagrange finite element function [32]

The two-level error satisfies

$$a(r_j, v - r_j) \ge p(v - r_j)\ \forall v \in \overline{\mathrm{K}}_{j+1}, \tag{36}$$

and residual p is defined as

$$p = l(v) - a(u_j, v_j) \tag{37}$$

With the help of triangle inequality and saturation assumption

$$(1-\hat{\lambda})\,||\,u - u_j\,|| \le ||\,r_j\,|| \le (1+\hat{\lambda})\,||\,u - u_j\,||$$

The contact problem is a nonlinear problem so it is solved iteratively. To calculate the two-level error we compute the stiffness matrices of the contact problem at a load step i. For the variational inequality, the linearized algebraic form of equation (36) is written as

$$\text{Find } u_j^i \in K_j : (K_j^i + K_{m,j}^i)\Delta u_j^i = f_j^i \tag{38}$$

Where, K_j^i is the consistent global matrix of dimension $\mathcal{N}_j^I \times \mathcal{N}_j^I$, and $K_{m,j}^i$ is the geometric tangential stiffness matrix which is a diagonal matrix of dimension $\mathcal{N}_j^C \times \dim(\mathcal{N}_j)$. Δu_j^i is the incremental displacement at load step *i*. Here $\mathcal{N}_j^I$ is the total number of mesh nodes which are not on contact boundary $\mathcal{N}_j^C$ is the number of nodes on the contact boundary and $\mathcal{N}_j$ is the total number of nodes at mesh resolution *j*. Using the multi-resolution and second generation wavelet customization, the algebraic equation at each iteration step has the form

$$\begin{bmatrix} S_0^s & & \cdot & \\ & D_1^D & \cdot & \cdot \\ \cdot & \cdot & \ddots & \cdot \\ & \cdot & \cdot & D_{j-1}^D \end{bmatrix}_i \begin{bmatrix} \Delta u_0^s \\ \Delta r_0 \\ \vdots \\ \Delta r_{j-1} \end{bmatrix}_i + \begin{bmatrix} (S_0^s)_c & & \cdot & \\ & (D_1^D)_c & \cdot & \cdot \\ \cdot & \cdot & \ddots & \cdot \\ & \cdot & \cdot & (D_{j-1}^D)_c \end{bmatrix}_i \begin{bmatrix} \Delta u_0^s \\ \Delta r_0 \\ \vdots \\ \Delta r_{j-1} \end{bmatrix}_i = \begin{bmatrix} f_0^s \\ f_0^D \\ \vdots \\ f_{j-1}^D \end{bmatrix}_i \tag{39}$$

We solve a small sub-system to calculate the wavelet detail

$$[D_1^D + (D_1^D)_C]_i (\Delta r_0)_i = (f_0^D)_i \tag{40}$$

A Hertz contact problem with the known analytical solution is considered to check the efficiency of our error estimator for variational inequalities[33]. The contact problem involves a frictionless contact condition between two infinitely long cylinders. The material is linearly elastic and isotropic, and deformation is considered infinitesimal with plane strain condition. For contact condition between a cylinder and a plane surface shown in figure 5, we assumed large values of radius R_2 and Young's modulus E_2 for the rigid surface. The Hertz analytical solution for the normal contact stress σ_n^H and the length b are given as [33]

$$\sigma_n^H(x) = \frac{4R_1 q}{\pi b^2}\sqrt{b^2 - x^2}$$

$$b = 2\sqrt{\frac{2R_1^2 q(1-\nu_1^2)}{E_1 \pi}}$$

We assumed Poisson's ratio ν_1 = 0.3, the radius of the cylinder R_1 = 8mm, Young's modulus E_1 = 80 GPa and the force applied to the structure F = 100 N. We compute the distributed load q = 625 N/m and the contact region b = 0.68077. The plane surface is taken as a rigid surface with a constrained lower edge. For the initial contact, closed gap condition is taken at the symmetry point of the cylinder.

Figure 5 shows the computational domain and a reduced model for simulation. The number of total nodes in the initial mesh is 150. Linear Dirichlet boundary condition is considered for non-contact points. The wavelet coefficients are estimated at each iteration step for local refinement. The normalized detail coefficients are measured in the energy norm[31].

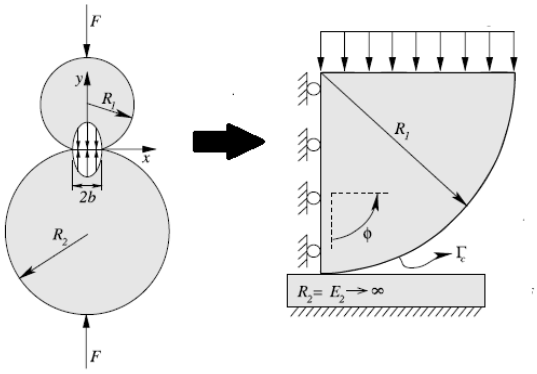

Figure 5: Two Cylinders in Contact and the Rigid-Deformable Approximation

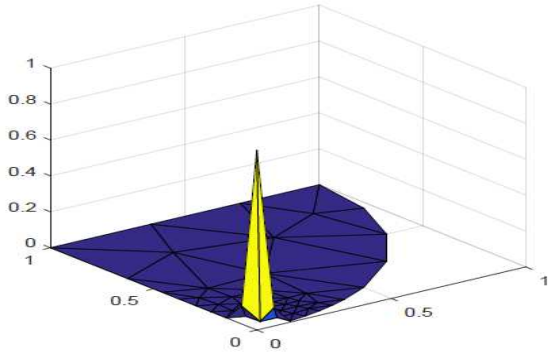

Figure 6: Amplitude of Normalized Wavelet Coefficients

The quantity of interest in this problem is maximum contact stress. The zone of interest in this problem is the elements around the neighborhood of contact point as the point of maximum stress lies on the contact boundary. The wavelet-based adaptive scheme is compared with uniform *h*-refinement of the computational mesh. An idealized equilibrated force system is applied at the contact interface. Figure 6 shows the distribution of details at refinement level 3; the wavelet coefficients show a peak over the elements with a maximum local error. The mesh is refined at the grid showing the high amplitude of wavelet detail.

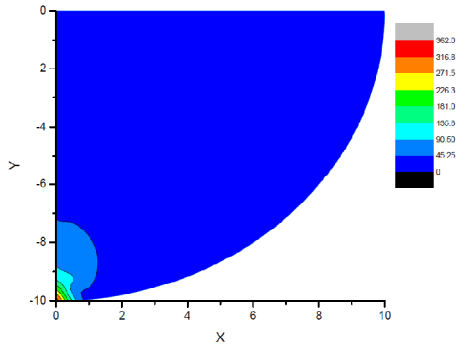

Figure 7: Von Mises Stress Distribution

Figure 7 shows the von Mises contact stress distribution at refinement level 3, and it can be observed the maximum contact stress is coming at the point of contact. Figure 8 shows a comparison between wavelet-based adaptive refinement and uniform refinement. it can be obsereved that for the same level of error reduction wavelet-based error indicator is more economical than uniform refinement.

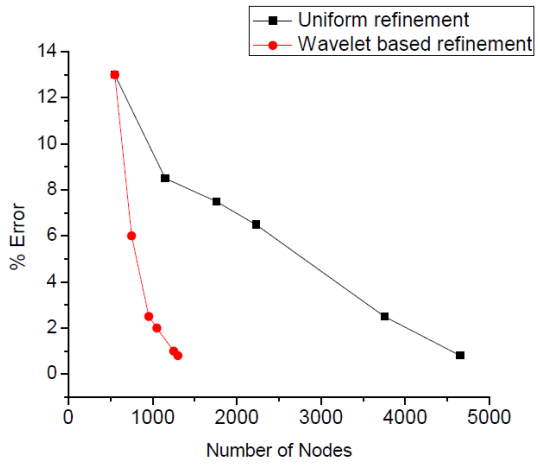

Figure 8: Comparison of Uniform vs. Wavelet-based Refinement

5. CONCLUSIONS

Accuracy, reliability, and computational cost are crucial issues of any efficient error estimator to design adaptive algorithms for the numerical solution of partial differential equations. The wavelet-based *a posteriori* error indicator is proposed to identify the location of grid refinement at a low computational cost to achieve an error bound solution for engineering problems. In this approach, the wavelet transform is used for error indicators that are easier and much simpler to implement than those available in the literature. Furthermore, it is locally efficient and can be used in complex engineering analysis with any finite element subspaces. Comparisons of the proposed estimator with exact error and two scale error with the help of numerical experiments show that it is as good as other error estimators. The key feature of the method is an automatic algorithm for any finite element grid structure. In situations where it might be impossible to directly verify the hypothesis, the findings of this study facilitate future researchers to advance the error estimation techniques. There are several areas in wavelet-based error estimator still needs research. This includes the selection of the most suitable wavelets for complex geometries with the large class of practical applications.

6. ACKNOWLEDGMENTS

This research did not receive any specific grant from funding agencies in the public, commercial, or not-for-profit sectors.

REFERENCES

1. *Babuska, W. C. Rheinboldt, A posteriori error analysis of finite element solutions for one-dimensional problems, SIAM J. Numer. Anal., 18 (1981).*
2. *R. Verfurth, A posteriori error estimation and adaptive mesh-refinement techniques, J. Comput. Appl. Math., 50 (1994) 67–83.*
3. *E. A. Bornemann, B. Erdmann, R. Kornhuber, A Posteriori Error Estimates For Elliptic Problems In Two And Three Space Dimensions, SIAM J. Numer. Anal., 33 (1996) 1188–1204.*
4. *M. Ainsworth, J. T. Oden, A posteriori error estimation in finite element analysis, Comput. Methods Appl. Mech. Eng., 7825 (1997).*
5. *Meyer, Error estimators and the adaptive finite element method on large strain deformation problems, Math. Methods Appl. Sci., 32 (2009) 2148–2159.*

6. *M. Li, S. Mao, S. Zhang, New error estimates of nonconforming mixed finite element methods for the Stokes problem, Math. Methods Appl. Sci., 37 (2014) 937–951.*
7. *L. Gao, D. Liang, B. Zhang, Error estimates for mixed finite element approximations of the viscoelasticity wave equation, Math. Methods Appl. Sci., 27 (2004) 1997–2016.*
8. *G. Kunert, A posteriori error estimation for convection dominated problems on anisotropic meshes, Math. Methods Appl. Sci., 26 (2003) 589–617.*
9. *P. M. Mohite, C. S. Upadhyay, Local quality of smoothening based a-posteriori error estimators for laminated plates under transverse loading, Comput. Struct., 80 (2002) 1477–1488.*
10. *T. Gratsch, K. J. Bathe, A posteriori error estimation techniques in practical finite element analysis, Comput. Struct., 83 (2005) 235–265.*
11. *E. Rabizadeh, A. Saboor, T. Rabczuk, Goal-oriented error estimation and adaptive mesh refinement in dynamic coupled thermoelasticity, Comput. Struct., 173 (2016) 187–211.*
12. *M. Guo, H. Zhong, Constitutive-relation-error-based a posteriori error bounds for a class of elliptic variational inequalities, Appl. Math. Lett., 71 (2017) 10–14.*
13. *P. Ladeveze, D. Leguillon, Error Estimate Procedure in the Finite Element Method and Applications, SIAM J. Numer. Anal., 20 (1983) 485–509.*
14. *V. H. Hoang, C. Schwab, High-Dimensional Finite Elements for Elliptic Problems with Multiple Scales, Multiscale Model. Simul., 3 (2005) 168–194.*
15. *F. Fierro, A. Veeser, A posteriori error estimators, gradient recovery by averaging, and superconvergence, Numer. Math., 103 (2006) 267–298.*
16. *R. Cottereau, P. Díez, A. Huerta, Strict error bounds for linear solid mechanics problems using a subdomain-based flux-free method, Comput. Mech., 44 (2009) 533–547.*
17. *K. H. Lee, Z. C. Xuan, Computing a-posteriori bounds for stress intensity factors in elastic fracture mechanics, Int. J. Fract., 126 (2004) 123–142.*
18. *F. Cirak, E. Ramm, A posteriori error estimation and adaptivity for linear elasticity using the reciprocal theorem, Comput. Methods Appl. Mech. Eng., 156 (1998) 351–362.*
19. *H. Yserentant, On the multi-level splitting of finite element spaces, Numer. Math., 49 (1986) 379–412.*
20. *R. E. Bank, T. F. Dupont, H. Yserentant, The Hierarchical Basis Multigrid Method, Numer. Math., 458 (1988) 427–458.*
21. *R. E. Bank, R. K. Smith, A posteriori error estimates based on hierarchical bases ∗, SIAM J. Numer. Anal., (1992) 1–15.*
22. *R. E. Bank, PLTMG: A Software Package for Solving Elliptic Partial Differential Equations, Society for Industrial and Applied Mathematics, 1998.*
23. *W. Sweldens, The Lifting Scheme: A Construction of Second Generation Wavelets, SIAM J. Math. Anal., 29 (1998) 511–546.*
24. *S. Bertoluzza, A Posteriori Error Estimates for the Wavelet Galerkin Method, Appl. Math. Lett., 8 (1995) 1–6.*
25. *Cohen, W. Dahmen, R. Devore, for Elliptic Operator Equations : Convergence Rates, 70 (2000) 27–75.*
26. *S. Dahlke, W. Dahmen, R. Hochmuth, R. Schneider, Stable multiscale bases and local error estimation for elliptic problems, Appl. Numer. Math., 23 (1997) 21–47.*

27. *K. Amaratunga, R. Sudarshan, Multiresolution modeling with operator-customized wavelets derived from finite elements, 195 (2006) 2509–2532.*

28. *R. E. Bank, A. Weiser, Some A Posteriori Error Estimators for Elliptic, (1984) 1–19.*

29. *R. K. R. K. O. Sander, P. D. S. Ertel, A monotone multigrid solver for two body contact problems in biomechanics, (2008) 3–15.*

30. *Mahadeshwar, A. M., Ghonge, A. S., & Chaudhari, K. A. Design, Development And Analysis Of Differential Anti-Reverse Mechanism.*

31. *S. Mallat, A Wavelet Tour of Signal Processing, 3rd Ed, Acad. Press. San Diego, (2008).*

32. *K. Amaratunga, R. Sudarshan, Multiresolution modeling with operator-customized wavelets derived from finite elements, Comput. Methods Appl. Mech. Eng., 195 (2006) 2509–2532.*

33. *R. Kornhuber, R. Krause, O. Sander, P. Deuflhard, S. Ertel, A monotone multigrid solver for two body contact problems in biomechanics, Comput. Vis. Sci., 11 (2008) 3–15.*

34. *R. G. Budynas, J. K. Nisbett, J. E. Shigley, Mechanical Engineering Design, McGraw-Hill, Singapore ;;London, 2008.*